International Symposium
On Turbulence and Shear Flow
Phenomena (TSFP-9)
June 30 - July 3, 2015 *Melbourne, Australia*

ASYMPTOTIC SIMILARITY STATES OF UNSTABLY STRATIFIED HOMOGENEOUS TURBULENCE

Alan Burlot
CEA, DAM, DIF, F-91297 Arpajon, France
alan.burlot@cea.fr

Benoît-Joseph Gréa
CEA, DAM, DIF, F-91297 Arpajon, France
benoit-joseph.grea@cea.fr

Fabien Godeferd
LMFA, Ecole centrale de Lyon, CNRS,
INSA, UCBL, F-69134 Ecully, France
fabien.godeferd@ec-lyon.fr

Claude Cambon
LMFA, Ecole centrale de Lyon, CNRS,
INSA, UCBL, F-69134 Ecully, France
claude.cambon@ec-lyon.fr

ABSTRACT

We study the late time dynamics of unstably stratified homogeneous turbulence (USHT) accounting for incompressible binary mixture under Boussinesq approximation. In order to explore the high Reynolds number regimes reached at long times, which cannot be represented in either laboratory experiments or direct numerical simulations, we use a spectral model based on the eddy damped quasi-normal Markovian (EDQNM) closure. We focus in this study on the dependence of the asymptotic regime on the large scale distribution specified in initial conditions, specified by the powerlaw scaling of the infrared spectral range. We are able to identify the various evolutions of kinetic energy corresponding to distinct self-similar states, characterized by the kinetic energy growth rate and the anisotropic structures created in the flow. Our results agree with recent theoretical predictions concerning USHT.

INTRODUCTION

The decay of homogeneous isotropic turbulence (HIT) is perhaps one the most studied topic in turbulence. While of fundamental importance, it is also the subject of intense theoretical debates illustrated by the question of permanence of big eddies related to the existence of invariants [Batchelor, 1953]. In situations where invariants exist, with a mostly downscale energy cascade — *i.e* backscatter terms are subdominant —, it is possible to relate the spectral powerlaw of the infrared range in the energy spectrum to the self-similar decay exponent of kinetic energy. This theoretical prediction was confirmed by Lesieur & Ossia [2000] using a spectral eddy damped quasi normal Markovian (EDQNM) simulations at high Reynolds number. Soulard *et al.* [2014] transposed these theoretical arguments to unstably stratified homogeneous turbulence (USHT) in order to evaluate the asymptotic growth rate of kinetic energy at sufficiently high Reynodlds number, therefore at long time. This brings to the fore the determinant role of the distribution of energy of the large-scale eddies, which, in spectral terms, translates in the powerlaw scaling k^s of the infrared range of kinetic energy spectrum $E(k)$, *i.e.*. at small wavenumbers k. One shows that the kinetic energy evolves self-similarly at late time as $\mathscr{K}(t) \sim e^{\beta N t}$, where N is the buoyancy frequency computed from the mean vertical density gradient and to the intensity of gravity (similar to the Brunt-Väisälä frequency in stably stratified flows). Using some hypotheses, Soulard *et al.* [2014] show that the growth rate β is related to the infrared slope as

$$\beta = \frac{4}{s+3}. \tag{1}$$

However, it is hard to confirm these predictions as the self-similar states of USHT are generally difficult to observe, due to a quickly increasing Reynolds number and to the permanent growth of turbulence structures fed by the buoyancy force. For instance, an important feature of USHT is the growth of the integral length scale which, at large time, generally induces confinement effects in experiments [Thoroddsen *et al.*, 1998] (due to the finite size of the container) and in direct numerical simulations (due to the periodicity of the domain in pseudo-spectral algorithms) [Griffond *et al.*, 2014]. In order to deal with this issue, we propose to extend the approach of Lesieur & Ossia [2000], for homogoeneous isotropic turbulence (HIT) modelled with an EDQNM closure, to the case of USHT. However, USHT dynamics is more complex than HIT dynamics since it is strongly anisotropic. This requires a significantly extended anisotropic EDQNM model which, in this work, follows the formalism introduced for axisymmetric turbulence by Godeferd & Cambon [1994] (see also Sagaut & Cambon [2008]). The EDQNM model dedicated to USHT has been successfully compared to several direct numerical simulations (DNS) at the available Reynolds numbers and with different parameters such as initial conditions for mixing intensity or strength of acceleration [Burlot *et al.*, 2015]. By studying self-similar states of USHT, we expect to gain a better insight into buoyancy induced turbulence which has many practical applications such as Rayleigh-Taylor mixing.

This article is organized as follows: first, we show the basic equations for USHT and briefly present the key elements of the EDQNM model. Then, we describe the different parametric simulations and discuss the characteristics of the self-similar late time dynamics.

BASIC EQUATIONS FOR UNSTABLY STRATIFIED HOMOGENEOUS TURBULENCE

The equations for unstably stratified flows derive from incompressible Navier-Stokes equations with Boussinesq assumption and express the dynamics of the fluctuating velocity field $\mathbf{u}$ in absence of mean velocity and of the fluctuating buoyancy field ϑ in presence of a vertical (along x_3) mean density gradient, as [Griffond *et al.*, 2014]

$$\frac{\partial u_i}{\partial x_i} = 0, \quad (2)$$

$$\frac{\partial u_i}{\partial t} + u_j \frac{\partial u_i}{\partial x_j} = -\frac{1}{\rho_0}\frac{\partial p}{\partial x_i} + \nu \frac{\partial^2 u_i}{\partial x_j \partial x_j} + N\vartheta\delta_{i3}, \quad (3)$$

$$\frac{\partial \vartheta}{\partial t} + u_j \frac{\partial \vartheta}{\partial x_j} = \mathscr{D}\frac{\partial^2 \vartheta}{\partial x_j \partial x_j} + Nu_3. \quad (4)$$

p is the pressure, ρ_0 a reference density, ν the kinematic viscosity, $\mathscr{D}$ the diffusion coefficient for buoyancy ϑ rescaled as a velocity. In practice, we restrict our study to unit Prandtl number such that $\nu = \mathscr{D}$. The buoyancy frequency N already introduced accounts for the strength of the acceleration and the mean stratification of the fluid. We assume here a uniform in space and constant in time N. The larger N the stronger stratification and/or gravity acceleration. Equation (2) states the incompressibility; Eqs. (3) and Eq. (4) show that the dynamics of the velocity field of the buoyancy field are coupled through two linear terms involving the destabilizing buoyancy force $\vartheta\delta_{i3}$ in Eq. (3), and Nu_3 in Eq. (4). Denoting the ensemble average $\langle\rangle$, velocity and buoyancy are such that $\langle u_i\rangle = \langle\vartheta\rangle = 0$ and their statistics are independent of the location in space from the homogeneous assumption.

Inverting the direction for the mean density gradient (*i.e.* replacing N by $-N$) in the USHT system permits to recover the stably stratified homogeneous turbulence (SSHT) case. First investigated by [Batchelor *et al.*, 1992], the unstable homogenenous case which we also consider here leads to buoyancy-induced turbulence which has been the subject of less studies than SSHT. USHT dynamics differs from SSHT dynamics due to the effect of buoyancy fluctuations steadily forced by N at all scales, which eventually leads to an exponential growth of kinetic energy, when N is constant. In Rayleigh-Taylor mixing, N varies slowly in time and yields different energy growth laws.

Eddy damped quasi normal model for unstably stratified homogeneous turbulence

In this section, we report some key aspects of the EDQNM closure used to investigate USHT. This model accounts for the dynamics of second-order correlations represented in spectral space. Due to axisymmetry, the spectra depend only on the modulus $k\,(\in[0\ +\infty])$ of the wavevector $\mathbf{k}$ and on the angle $\theta\,(\in[0\ \pi])$ between $\mathbf{k}$ and the vertical direction. Also for symmetry reasons, the tensorial structure of the spectral two-point velocity auto-correlation tensor and velocity-buoyancy tensor reduces to four scalar spectra $\Phi_1(k,\theta,t)$, $\Phi_2(k,\theta,t)$, $\Phi_3(k,\theta,t)$ and $\Psi_r(k,\theta,t)$ representing respectively toroidal and poloidal kinetic energy, buoyancy scalar spectrum and co-spectrum between poloidal velocity and buoyancy scalar [Godeferd & Cambon, 1994]. This yields the following system of equations which takes advantage of a representation in the polar-spherical frame of reference in spectral space, also called the Craya-Herring frame:

$$\left(\frac{\partial}{\partial t} + 2\nu k^2\right)\Phi_1 = T^{\Phi_1}, \quad (5)$$

$$\left(\frac{\partial}{\partial t} + 2\nu k^2\right)\Phi_2 = T^{\Phi_2} + 2N\sin(\theta)\Psi_r, \quad (6)$$

$$\left(\frac{\partial}{\partial t} + 2\nu k^2\right)\Phi_3 = T^{\Phi_3} + 2N\sin(\theta)\Psi_r, \quad (7)$$

$$\left(\frac{\partial}{\partial t} + 2\nu k^2\right)\Psi_r = T^{\Psi_r} + N\sin(\theta)\left(\Phi_2 + \Phi_3\right). \quad (8)$$

In Eqs. (5)–(8), left hand side shows the dynamics and viscous/diffusion contributions. In the right-hand side, linear terms proportional to N stand for buoyancy effects while the different non linear transfer terms noted $T^{\Phi_1,\Phi_2,\Phi_3,\Psi_r}$ (depending also on k, θ and t) are expressed by two-point third-order correlations evaluated from the four above two-point statistical spectra following the EDQNM closure. Stratification effects are specifically taken into account in the closure for these triple correlations by including the buoyancy timescale $1/N$ along with the turbulence timescale in the eddy damping. Including the buoyancy time scale in the model for energy transfer terms was shown to be indispensable for the model to be able to reproduce accurately USHT DNS [Burlot *et al.*, 2015]. The EDQNM model has thus been successfully tested against relevant configurations with different acceleration strengths and mixing intensities. It is worth mentioning that, due to the anisotropic structure of spectra, the implementation of our EDQNM model is much more complex than that of isotropic EDQNM. However, this complexity allows the EDQNM model to reproduce DNS results at a much lower computational cost, and to reach very high Reynolds number regimes unattainable by DNS, as shown in the coming section.

RESULTS

In this section, we detail the simulations carried out to evaluate the late time regimes of USHT. Then, we present and discuss the different results.

Configurations

We choose initial isotropic conditions for the different EDQNM simulations. Accordingly, the different spectra at $t = 0$ have no dependence on θ, the toroidal spectrum equals the poloidal one ($\Phi_1 = \Phi_2$) and the co-spectrum Ψ_r is zero. Also for simplicity, the buoyancy scalar spectrum is initially taken at the same level as other spectra such that $\Phi_3 = \Phi_1 = \Phi_2$. The initial energy spectrum $E(k) = \int_0^\pi 2\pi k^2 \sin(\theta)\left(\frac{\Phi_1+\Phi_2}{2}\right)d\theta$ is similar to the one used by [Lesieur & Ossia, 2000], namely:

$$E(k,t=0) = A\left(\frac{k}{k_{peak}}\right)^s \exp\left[-\frac{s}{2}\left(\frac{k}{k_{peak}}\right)^2\right]. \quad (9)$$

In Eq. (9), the parameter s gives the slope of infrared spectra which controls the repartition of energy at large scales. It varies from $s = 1$ to $s = 5$ in our ten different simulations as indicated in Tab. 1. In each simulation, we impose the same initial values for the kinetic energy $\mathscr{K} = \int_0^{+\infty} E(k,0)\,\mathrm{d}k = 1$ and viscosity $\nu = 5\times10^{-4}$. Therefore, k_{peak} corresponds

Table 1. Characteristics of the different EDQNM cases presented in this work: powerlaw s, peak wavenumber k_{peak}, total kinetic energy $\mathscr{K}$, Reynolds number Re, Froude number Fr.

s	k_{peak}	$\mathscr{K}$	Re	Fr
1	34.64	1	834	1.2
1.5	37.95	1	834	1.2
2	40.00	1	834	1.2
2.5	41.40	1	834	1.2
3	42.43	1	834	1.2
3.5	43.20	1	834	1.2
4	43.82	1	834	1.2
4.5	44.32	1	834	1.2
5	44.72	1	834	1.2

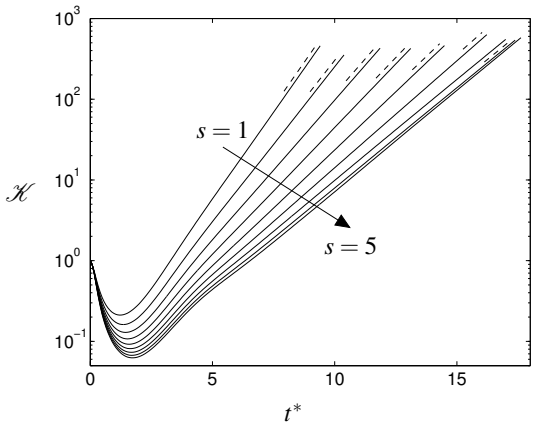

Figure 1. Time evolution of the kinetic energy with respect to non dimensional time $t^* = Nt$. Each curve corresponds to different initial infrared exponent s. The slopes for the different dashed straight lines corresponds to the theoretical $\beta(s)$ of Eq. (1).

to the wavenumber at the maximum of the spectrum, and A is adjusted in Eq. (9) in order to keep constant the initial Reynolds number $Re = \mathscr{K}^2/(\varepsilon\nu)$ (ε being the kinetic energy dissipation).

We specify initially the buoyancy frequency N for each USHT simulations. The different cases are characterized by the Froude number, $Fr = \varepsilon/(N\mathscr{K})$, measuring the relative importance of buoyancy forces with respect to inertial forces. We choose a constant initial Froude number $Fr = 1.2$ in all our simulations so that stratification effects are relatively moderate initially, but increase rapidly in time.

Dynamics and energetics of USHT

We show in Figure 1 the time evolution of kinetic energy in the different EDQNM simulations. After some transients, whose duration Δt depends on initial conditions ($N\Delta t \sim 2-4$), the flow enters a self-similar regime and kinetic energy grows exponentially $\sim e^{\beta Nt}$. As already mentioned in Eq. (1), the growth rate β strongly depends on the initial distribution at large scale of energy in the turbulent eddies. Two different situations are observed, similar to what happens in HIT. For $s \leq 4$, the growth rate β is perfectly predicted by Eq. (1). For $s > 4$, the slope of the infrared spectrum evolves during a transient short time stage under the action of backscatter effects, to finally set at the value $s = 4$, which is later maintained. These results confirm the theory proposed by [Soulard *et al.*, 2014] which assumes the dominance of non-local interactions between wavenumbers at small k.

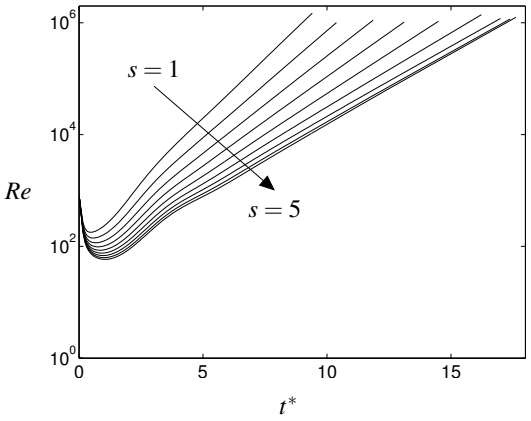

Figure 2. Evolution of turbulent Reynolds number as a function of time for the different cases of Tab. 1.

Figure 2 shows the evolution of the Reynolds number as a function of time. It shows the same evolution as kinetic energy in the self-similar state. Globally, these self-similar states are observed for $Re > 10^3$ and are maintained until the end of the simulations around $Re \sim 10^6$. As in Figure 1, a transient phase is noticed with two stages: a relative decrease of the Reynolds number followed by a temporary growth leading to the self-similar state. The intensity of the decrease is clearly dependent on the initial energy distribution at large scales.

In Figure 3, we observe the time evolution of the Froude number. It converges to stationary values in the range $Fr \in [0.3, 0.5]$, values which also depends on initial conditions. The initial slope at large scale tends to drive the Froude number to different values. If the initial energy is preferentially distributed at larges scales, i.e. small s value, the asymptotic value of the Froude number will be smaller. The nearly steady behavior of the Froude number does not arise at the same time as for the Reynolds number. A bump is observed for large values of s, which disappears progressively until the asymptotic value of Froude number is reached. This sheds light on the different evolutions of dissipation and kinetic energy depending on the initial energy distribution: the cascading time for energy from the energetic scales to the dissipative ones depends on s. The fact that, when the similarity state is reached, the Froude number do not evolve anymore attests of an equilibrium between the vertical motion of large scale structures, driven by the buoyancy force, and the drag they encounter. This is all the more remarkable in the homogeneous case in which no external length scale imposes a limit, with respect to actual flows in which the physical domain limits the structures' size growth. Moreover, the value reached by the Froude

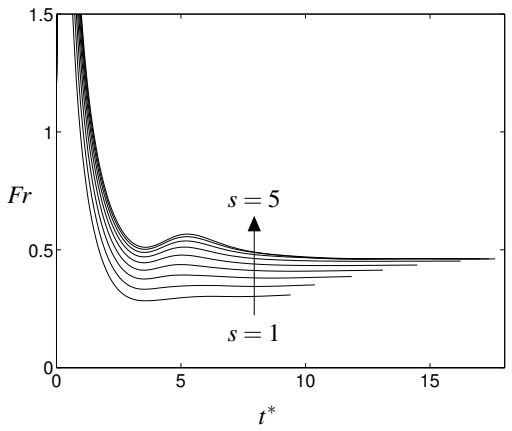

Figure 3. Evolution of the Froude number as a function of time for the different cases of Tab. 1.

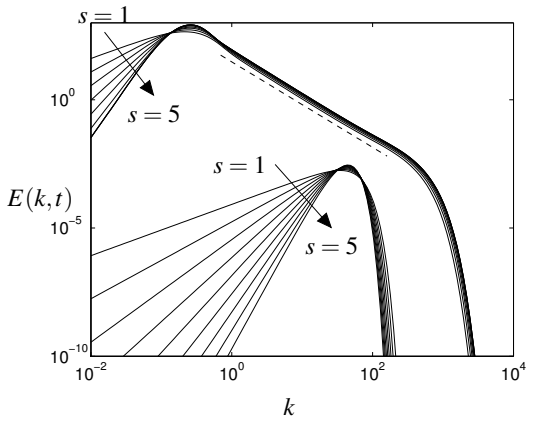

Figure 4. Spectra of kinetic energy at initial time and at the time corresponding to a given Reynolds number ($\simeq 10^6$). Initial spectra shifted a decade down for clarity.

number is smaller than one but not very small, attesting of the equilibrium between nonlinear turbulent timescale and the linear production timescale of buoyancy.

The energy spectra for the different cases are represented in Figure 4 both at $t = 0$ and at a time corresponding to $Re \simeq 10^6$ in each simulation. It can be noticed that the different self-similar regimes exhibit a clear well developed $k^{-5/3}$ inertial range over two decades. Also, it illustrates the backscatter effects which modify the slope of the infrared range of the spectra for cases with $s > 4$. The evolution of the spectra for the different s cases shows that energy uniformly increases throughout the scales from the initial states, but also that the very important changes in the spectral shape that occur in the large scales have very few influence on the rest of the distribution, in the inertial and dissipative ranges. We therefore observe here the fact that the buoyancy force acts onto all scales, but that nonlinear cascade remains dominant and yields a Kolmogorov scaling, independently on the initial conditions.

Characterization of anisotropy

It is clear that the structure of the velocity field in USHT is strongly coupled to the vertical events occuring in the flow, so that we expect turbulent structures to be vertically oriented and elongated, as in convective turbulence, but also that the fluctuating buoyancy field also exhibit strongly anisotropic features. This translates in spectral space through the dependence of the kinetic energy and buoyancy scalar spectra with the orientation θ of the wavevector, since incompressibility amounts to $\mathbf{k}\cdot\hat{\mathbf{u}} = 0$, so that preferentially vertical velocity is associated with horizontal wavevectors. Correspondingly, kinetic energy spectra have more energy in the horizontal orientations of $\mathbf{k}$, at $\theta \simeq \pi/2$. Please also note that the EDQNM model is particularly well suited for this kind of analysis, since its equations directly operate on the (k,θ)–dependent spectra, whereas the same statistics from DNS require averaging and are subjected to sampling biases.

We begin by examining the anisotropy of the Reynolds stress tensor that can be measured by its vertical deviatoric part $b_{33} = \langle u_3 u_3\rangle / \langle u_i u_i\rangle - 1/3$, whose time evolution is represented in Figure 5. Starting from isotropic turbulence for which $b_{33} = 0$, we observe a rapid increase of b_{33} within one or two stratification timescales. After this transient, b_{33} reaches an asymptotic value of 0.3 for the case of steeper infrared powerlaw $s = 5$, but for the case of shallow infrared powerlaw $s = 1$ b_{33} slowly drifts away from the peak 0.4 value, so that the flow becomes more and more anisotropic. This may be due to local interactions that progressively propagate anisotropy from the highly anisotropic large scales to smaller inertial scales. Whether an asymptotic limit is reached is an open question, but, our simulations seem to suggest that it would only occur at very long times for which the Reynolds number would become huge.

Concerning the characterization of the buoyancy scalar spectrum, buoyancy being a scalar field, one cannot compute an equivalent to the velocity two-point correlation anisotropy which is based on its components. Therefore, we choose to characterize the anisotropy of the buoyancy scalar spectrum by the *dimensionality* parameter introduced by Gréa [2013], which is based on a weighted integral as

$$\sin^2\gamma = \frac{\int_0^\pi \int_0^{+\infty} k^2 \sin^3(\theta)\Phi_3 dk d\theta}{\int_0^\pi \int_0^{+\infty} k^2 \sin(\theta)\Phi_3 dk d\theta} \,. \qquad (10)$$

Similar integrals are used in magnetohydrodynamics to quantify the flow anisotropy through a Shebalin angle. Here, the angle γ represents the angle of concentration of buoyancy scalar fluctuations in the neighborhood of the vertical direction. Then, as for b_{33} for the velocity field, we observe a short-time transient during which $\sin^2\gamma$ increases, although not as fast. At longer times, the evolution is much slower for the case at $s = 5$ than for the case at $s = 1$. Note that the anisotropy level varies a lot with s when $s < 4$, but much less for $s \geq 4$. This also attests of a different nature in the dynamics, for wich backscatter is present in the latter case but not in the former. In all cases however, the value of $\sin^2\gamma > 2/3$ indicates the presence of vertical patches of density concentration, more elongated for low infrared spectral slopes.

CONCLUSION

The USHT late time self-similar dynamics are investigated with an axisymmetric EDQNM model. The model permits to reach very high Reynolds numbers $Re \sim O(10^6)$ out of reach of DNS, and this is especially useful for studying the large-time asymptotic dynamics of USHT whose

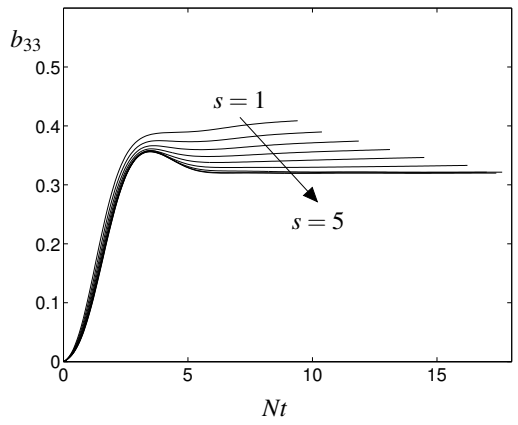

Figure 5. Time evolution of the vertical deviatoric part of the Reynolds stress tensor b_{33}.

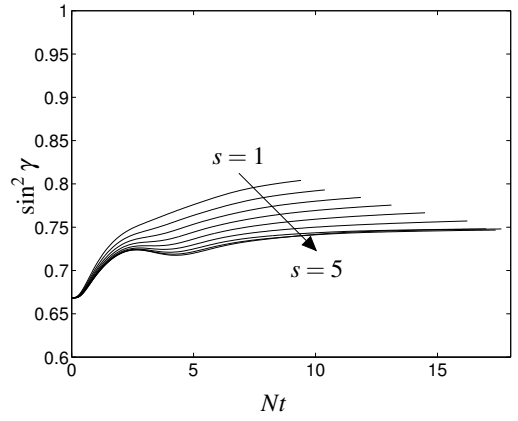

Figure 6. Time evolution of the dimensionality parameter $\sin^2\gamma$ measuring anisotropy of the buoyancy parameter.

energy increases quickly since it is fed by the buyoancy force-related production. Our results confirm recent theoretical predictions for USHT pertaining to the link between the growth rate and the initial distribution of kinetic energy at large scale. It also brings additional insight into the differences of anisotropy structure appearing in the flow due to initial conditions. An original result is that the Froude number evolves in time to become asymptotically steady and sets at a value of order 0.3–0.5, for our set of initial parameters. This is a clue that an equilibrium is reached between linear production and nonlinear cascade, and opens the way to an improved modelling such as the drag-production one-point model, including a dependence on big eddies distribution.

Unstably stratified turbulence is a simplified model for phenomena that are observed in more complex situations, such as Rayleigh-Taylor mixing. Our work shows that one can link the large-time growth of the mixing layer to the nature or wavelength of the initial instabilities that trigger turbulence in Rayleigh-Taylor flows. Hence, this opens new possibilities for understanding and predicting the evolution of turbulent mixing layers induced by buoyancy effects. In order to confer more relevance to our approach, our next step will be to introduce time-dependent buoyancy parameter N, since the mean density gradient evolves in time in non homogeneous mixing layers.

REFERENCES

Batchelor, G. K. 1953 *The Theory of Homogeneous Turbulence*. Cambridge University Press.

Batchelor, G. K, Canuto, V. M. & Chasnov, J. R. 1992 Buoyancy-driven variable-density turbulence. *Journal of Fluid Mechanics* **235**, 349–378.

Burlot, A., Gréa, B.-J., Godeferd, F. S., Cambon, C. & Griffond, J. 2015 Spectral modelling of high reynolds number unstably stratified homogeneous turbulence. *Journal of Fluid Mechanics* **765**, 17–44.

Godeferd, F. S. & Cambon, C. 1994 Detailed investigation of energy transfers in homogeneous stratified turbulence. *Physics of Fluids* **6** (6), 2084–2100.

Gréa, B.-J. 2013 The rapid acceleration model and growth rate of a tubulent mixing zone induced by Rayleigh-Taylor instability. *Phys. Fluids* **25**, 015118.

Griffond, J., Gréa, B.-J. & O., Soulard. 2014 Unstably stratified homogeneous turbulence as a tool for turbulent mixing modeling. *J. Fluids Eng.* **136**, 091201.

Lesieur, M. & Ossia, S. 2000 3d isotropic turbulence at very high Reynolds numbers: EDQNM study. *J. of Turb.* **1**, N7.

Sagaut, P. & Cambon, C. 2008 *Homogeneous Turbulence Dynamics*. Cambridge University Press.

Soulard, O., Griffond, J. & Gréa, B.-J. 2014 Large-scale analysis of self-similar unstably stratified homogeneous turbulence. *Phys. Fluids* **26**, 015110.

Thoroddsen, S. T., Van Atta, C. W. & Yampolsky, J. S. 1998 Experiments on homogeneous turbulence in an unstably stratified fluid. *Physics of Fluids* **10** (12), 3155–3167.